ISSN 1063-7788, Physics of Atomic Nuclei, 2010, Vol. 73, No. 7, pp. 1152–1163. © Pleiades Publishing, Ltd., 2010.
Original Russian Text © V.Yu. Denisov, N.A. Pilipenko, 2010, published in Yadernaya Fizika, 2010, Vol. 73, No. 7, pp. 1191–1202.

NUCLEI
Theory

Interaction and Fusion of Deformed Nuclei

V. Yu. Denisov* **and N. A. Pilipenko**

Institute for Nuclear Research, National Academy of Sciences of Ukraine, pr. Nauki 47, 03680, Kyiv, Ukraine

Received July 24, 2009; in final form, December 9, 2009

Abstract—It is shown that the height of the barrier and its position, as well the depth of the capture well, are highly sensitive to the relative orientation of colliding strongly deformed nuclei. It is found that the fusion/capture cross sections and the nucleus–nucleus potential for heavy nuclear systems depend greatly on the magnitude and sign of the quadrupole deformation of nuclear surfaces. In order to describe correctly the cross section for the capture of heavy strongly deformed nuclei, it is necessary to perform averaging over all three angles that describe their relative orientation. Allowance for a hexadecapole deformation leads to a significant increase in the capture cross section for very heavy nucleus–nucleus systems.

DOI: 10.1134/S1063778810070082

1. INTRODUCTION

The fusion of nuclei is widely used in nuclear physics to produce nuclei far off the beta-stability line and superheavy nuclei, to explore the properties of excited nuclear states and the mechanisms of their decay, and to study the dynamics of nuclear reactions [1–6]. The burning of stars is also associated with reactions involving the subbarrier fusion of nuclei [7]. Nuclei studied thus far are mostly deformed. Deformed nuclei are frequently used in experimentally studying various nuclear reactions and are involved in nuclear reactions proceeding in stars [8]. Therefore, investigation of reactions between deformed nuclei at energies in the vicinity of the barrier is of great topical interest.

In studying in detail subbarrier-fusion reactions, the respective cross sections were found to exceed considerably the predictions of the model of one-dimensional tunneling. Various models and mechanisms of fusion reactions were proposed for describing a considerable enhancement of the cross section at subbarrier energies (see [5, 6, 8–22] and references therein).

The orientation of deformed nuclei affects significantly the barrier height [9, 13, 14, 17, 22–25] and the shape of the capture well in the nucleus–nucleus potential [25]. By way of example, we indicate that, in reactions between the spherical nucleus ^{48}Ca and the deformed heavy nuclei ^{238}U, ^{244}Pu, and ^{248}Cm—one employs these reactions to produce superheavy nuclei [26]—the change in the barrier height in response to changes in orientation may be as large as some 20 MeV [24]. Variations in the barrier height for different orientations of two deformed heavy nuclei are still greater [25].

The cross section for the fusion of nuclei at energies in the vicinity of the barrier depends greatly on the barrier height; therefore, orientation effects are of importance for correctly calculating the cross section for the fusion of deformed nuclei.

Our study reported in [25] was devoted to studying in detail and calculating the potential of the interaction of deformed nuclei for various orientations. In Section 2 of the present article, the approximations used in calculating the Coulomb and nuclear interactions between deformed nuclei are therefore described only briefly. A model for calculating the cross section for the fusion of deformed nuclei is formulated in Section 3. In Section 4, the interaction potentials and the fusion/capture cross section are analyzed in detail for various systems of deformed nuclei.

2. INTERACTION OF DEFORMED NUCLEI

The relative orientation of two deformed arbitrarily oriented axisymmetric nuclei in space is determined by the angles Θ_1, Θ_2, and Φ (see Fig. 1). With allowance for all linear and quadratic terms in the quadrupole deformation (β_2) and linear terms in higher deformations ($\beta_{L>2}$) of colliding nuclei, the Coulomb interaction of two deformed nuclei can be represented in the form [25]

$$V_{\rm C}(R,\Theta_1,\Theta_2,\Phi) \qquad (1)$$
$$= \frac{Z_1Z_2e^2}{R}\Bigg\{1+\sum_{L\geq 2}[f_{1L}(R,\Theta_1,R_{10})\beta_{1L} + f_{1L}(R,\Theta_2,R_{20})\beta_{2L}]$$

*E-mail: denisov@kinr.kiev.ua

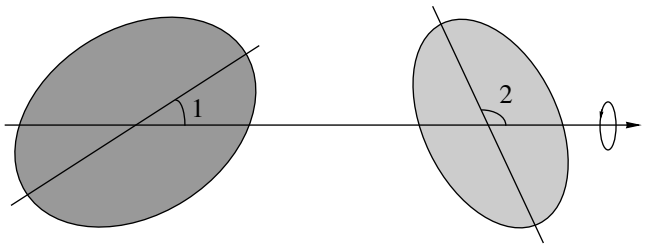

Fig. 1. Angles Θ_1, Θ_2, and Φ describing the relative orientation of deformed nuclei.

$$+ f_2(R,\Theta_1,R_{10})\beta_{12}^2 + f_2(R,\Theta_2,R_{20})\beta_{22}^2 + f_3(R,\Theta_1,\Theta_2,R_{10},R_{20})\beta_{12}\beta_{22} + f_4(R,\Theta_1,\Theta_2,\Phi,R_{10},R_{20})\beta_{12}\beta_{22}\Big\}.$$

Here, Z_1 and Z_2 are the numbers of, respectively, protons and neutrons in the corresponding nucleus; e is the proton charge; R is distance between the centers of mass of colliding nuclei; R_{i0} is the radius of the ith nucleus, while β_{iL} is the magnitude of the L-pole deformation in it;

$$f_{1L}(R,\Theta_i,R_{i0}) = \frac{3R_{i0}^L}{(2L+1)R^L}Y_{L0}(\Theta_i),$$

$$f_2(R,\Theta_i,R_{i0}) = \frac{6\sqrt{5}R_{i0}^2}{35\sqrt{\pi}R^2}Y_{20}(\Theta_i) + \frac{3R_{i0}^4}{7\sqrt{\pi}R^4}Y_{40}(\Theta_i),$$

$$f_3(R,\Theta_1,\Theta_2,R_{10},R_{20}) = \frac{27R_{10}^2R_{20}^2}{80\pi R^4}[17\cos^2(\Theta_1)\cos^2(\Theta_2) - 5\cos^2(\Theta_1) - 5\cos^2(\Theta_2) + 1],$$

$$f_4(R,\Theta_1,\Theta_2,\Phi,R_{10},R_{20}) = \frac{27R_{10}^2R_{20}^2}{40\pi R^4}[\cos^2(\Phi)\sin^2(\Theta_1)\sin^2(\Theta_2) - 2\cos(\Phi)\sin(2\Theta_1)\sin(2\Theta_2)];$$

and $Y_{L0}(\Theta)$ is the spherical harmonic of multipole order L.

We note that, as a rule, the quadrupole deformation and higher deformations of nuclei satisfy the relation $\beta_2^2 \approx \beta_{L>2}$; therefore, the formula that takes simultaneously into account all terms that are linear and quadratic in quadrupole deformations of nuclei and terms that are linear in their higher deformations is an expression accurate to order β_2^2 inclusive, while the next correction terms of order β_2^3 (or $\beta_2\beta_{L>2}$) are negligible at realistic values of nuclear deformations.

Also, a method for calculating the nuclear part of the interaction $V_N(R,\Theta_1,\Theta_2,\Phi)$ of two deformed nuclei with allowance for all terms that linear and quadratic in the quadrupole deformation and terms that are linear in higher deformations of colliding nuclei was proposed in [25]. This method is based on the analytic form obtained for the potential $V_{N\mathrm{sph}}(d)$ [27] upon fitting 7140 potentials representing the interaction between various spherical nuclei and emerging from calculations performed in the extended Thomas–Fermi approximation with the SkM^* Skyrme forces by using frozen proton and neutron densities in colliding nuclei, these proton and neutron densities being found in the Hartree–Fock–Bardeen–Cooper–Schrieffer approximation with the SkM^* Skyrme forces. We note that the results obtained for the heights and radii of the barriers with the aid of the analytic parametrization of $V_{N\mathrm{sph}}(d)$ for spherical nuclei agree well with the corresponding experimental values from [27, 28]. In order to take into account the effect of deformations on the strength of the nuclear interaction between the surfaces of colliding nuclei, we used the "proximity" theorem [29]. In this case, the potential of nuclear interaction between deformed nuclei is related to the potential of interaction between spherical nuclei by an equation of the form

$$V_N(R,\Theta_1,\Theta_2,\Phi) \approx \frac{1/R_{10}+1/R_{20}}{\left[(C_1^{||}+C_2^{||})(C_1^{\perp}+C_2^{\perp})\right]^{1/2}} \times V_{N\mathrm{sph}}(d(R,\Theta_1,\Theta_2,\Phi,R_{10},R_{20},\beta_{12},\beta_{22},\beta_{1L},\beta_{2L})), \quad (2)$$

where $V_{N\mathrm{sph}}(d)$ is the nuclear part of the interaction as found for spherical nuclei by formulas from [27] for the distance $d = d(R_{\mathrm{sph}} - R_{10} - R_{20}) = R_{\mathrm{sph}} - R_{10} - R_{20}$ between the surfaces of the nuclei, R_{sph} being the distance between the centers of the interacting nuclei; R_{10} and R_{20} are the radii of the interacting nuclei; and $C_i^{||}$ and $C_i^{\perp}$ are the principal curvatures of the deformed surface of a nucleus at the point closest to the surface of the other nucleus. The formulas for calculating the principal curvatures

of a deformed nucleus were derived in [25] with allowance for all terms that are linear and quadratic for the quadrupole deformation (β_2) and the terms that are linear in higher deformations ($\beta_{L>2}$) of the nuclear surface. In view of the importance of knowing, to the highest possible accuracy, the minimum distance $d(R, \Theta_1, \Theta_2, \Phi, R_{10}, R_{20}, \beta_{12}, \beta_{22}, \beta_{1L}, \beta_{2L})$ between the deformed surfaces for calculating the potential [23, 30], this distance was determined precisely by numerical methods.

At any point of the surface of a spherical nucleus, the principal curvatures are $C^{||} = C^{\perp} = 1/R_0$, where R_0 is the radius of this surface. It follows that, in the limit of negligible deformations, expression (2) for the potential of deformed nuclei also describes the potential of spherical nuclei.

For various orientations of a deformed nucleus, the difference of the results found numerically and with the aid of the above approximate expressions (1) and (2) for the potentials of a spherical and a strongly deformed nucleus, $V_C(R, \Theta_1, \Theta_2, \Phi) + V_N(R, \Theta_1, \Theta_2, \Phi)$, is less than 1% in the vicinity of the barrier [24], and this is indicative of a high accuracy of the proposed method for calculating the potential.

The terms that are quadratic in the deformation of nuclei contribute to the potential of interaction between very heavy nuclei [25]. Therefore, it would be useful to calculate the cross section for the fusion of two deformed nuclei as a function of deformation in the vicinity of the barrier by using the nucleus–nucleus potential from [25]. In this case, one could clarify the effect of the terms that are quadratic in the quadrupole deformation of nuclei on the fusion cross section, as well as the dependence of the fusion cross section on the deformation type (prolate, $\beta_{i2} > 0$, versus oblate, $\beta_{i2} < 0$) and on the masses and charges of interacting nuclei.

It should be noted that reactions involving the fusion of deformed nuclei were studied in [9, 13, 14]. In the calculation of the nucleus–nucleus potential in [13, 14], only the terms that are linear in the quadrupole deformation of nuclei (that is, terms proportional to β_{i2}) were taken into account. In [9], not all of the terms that are quadratic in the quadrupole deformation (β_{i2}^2) were taken into account in calculating the Coulomb interaction of deformed nuclei; also, crossed terms proportional to $\beta_{12}\beta_{22}$ were discarded there. We indicate that the crossed terms proportional to $\beta_{12}\beta_{22}$ determine the interaction potential as a function of the angles Θ_1, Θ_2, and Φ.

3. FUSION OF DEFORMED NUCLEI

Various relative orientations are possible for colliding nuclei; therefore, it is necessary to average the cross section over all possible orientations of deformed nuclei. Thus, we have

$$\sigma(E) = \frac{\pi\hbar^2}{2\mu E}\sum_{\ell}(2\ell+1) \tag{3}$$
$$\times \langle T(E, \ell, \Theta_1, \Theta_2, \Phi)\rangle = \frac{\pi\hbar^2}{2\mu E}\sum_{\ell}(2\ell+1)$$
$$\times \frac{1}{8\pi}\int_0^{\pi}\sin(\Theta_1)d\Theta_1\int_0^{\pi}\sin(\Theta_2)d\Theta_2$$
$$\times \int_0^{2\pi} d\Phi T(E, \ell, \Theta_1, \Theta_2, \Phi).$$

Here, $T(E, \ell, \Theta_1, \Theta_2, \Phi)$ is the transmission coefficient that describes the penetration through the barrier and which one calculates at a collision energy E and for the relative orientation of nuclei that is specified by the angles Θ_1, Θ_2, and Φ; ℓ is the relative orbital angular momentum of colliding nuclei; and angular brackets denote averaging over the relative orientations of the nuclei involved.

We note that, as nuclei approach each other, they can slightly rotate owing to the effect of Coulomb and nuclear forces. For example, the long-range Coulomb potential at a given distance between prolate nuclei has a minimum value at $\Theta_1 = \Theta_2 = 90^\circ$ [25, 31]; therefore, the Coulomb interaction tends to increase the angles Θ_1 and Θ_2 at the stage of approach and to render them closer to $\Theta_1 = \Theta_2 = 90^\circ$. On the contrary, the short-range nuclear interaction pushes the orientation of prolate nuclei toward $\Theta_1 = \Theta_2 = 0^\circ$. However, calculations reveal that variations in angles as the nuclei approach each other can be neglected since they are about a few degrees.

For subbarrier collision energies, we will use the transmission coefficient determined in the Wentzel–Kramers–Brillouin approximation [32]. In this case, the transmission coefficient has the form

$$T(E, \ell, \Theta_1, \Theta_2, \Phi) = \left\{1 + \exp\left[\frac{2}{\hbar}\int_{a(E,\ell,\Theta_1,\Theta_2,\Phi)}^{b(E,\ell,\Theta_1,\Theta_2,\Phi)}\sqrt{2\mu[V(R, \ell, \Theta_1, \Theta_2, \Phi) - E]}dR\right]\right\}^{-1}, \tag{4}$$

where $a(E,\ell,\Theta_1,\Theta_2,\Phi)$ and $b(E,\ell,\Theta_1,\Theta_2,\Phi)$ are, respectively, the inner and outer turning points; μ is the reduced mass of nuclei;

$$V(R,\ell,\Theta_1,\Theta_2,\Phi) = V_C(R,\Theta_1,\Theta_2,\Phi) + \eta V_N(R,\Theta_1,\Theta_2,\Phi) + \frac{\hbar^2\ell(\ell+1)}{2\mu R^2} \quad (5)$$

is the total nucleus–nucleus interaction potential calculated at the distance R between the centers of mass of the nuclei and for the relative orientation of nuclei that is specified by the angles Θ_1, Θ_2, and Φ; and η is an adjustable coefficient that determines the contribution of the nuclear potential component $V_N(R,\Theta_1,\Theta_2,\Phi)$ to the total potential. The inner and outer turning points are determined from the conditions $V(a(E,\ell,\Theta_1,\Theta_2,\Phi),\ell,\Theta_1,\Theta_2,\Phi) = E$ and $V(b(E,\ell,\Theta_1,\Theta_2,\Phi),\ell,\Theta_1,\Theta_2,\Phi) = E$, respectively.

At collision energies above the barrier, the transmission coefficient is determined by the Hill–Wheeler expression [33]

$$T(E,\ell,\Theta_1,\Theta_2,\Phi) = \left\{1+\exp\left[2\pi\frac{V_{\rm bar}(\ell,\Theta_1,\Theta_2,\Phi)-E}{\hbar\Omega}\right]\right\}^{-1}, \quad (6)$$

which takes into account the above-barrier reflection from a parabolic barrier. Since the height $V_{\rm bar}(\ell,\Theta_1,\Theta_2,\Phi)$ of the barrier, its curvature

$$\hbar\Omega = \sqrt{-\frac{\hbar^2}{\mu}\frac{d^2V(r,\ell,\Theta_1,\Theta_2,\Phi)}{dr^2}}\Bigg|_{r=R_{\rm bar}(\ell,\Theta_1,\Theta_2,\Phi)},$$

and its position $R_{\rm bar}(\ell,\Theta_1,\Theta_2,\Phi)$ depend significantly on the orientation of the nuclei—that is, on the angles Θ_1, Θ_2, and Φ—and on the orbital angular momentum ℓ of nuclei, the transmission coefficient calculated with the aid of Eq. (4) or (6) also depends strongly on the relative orientation of nuclei and on ℓ.

With the aid of formulas (1) and (2) and formulas from [25], the potential $V(R,\ell,\Theta_1,\Theta_2,\Phi)$ and the height of the barrier can easily be calculated for any relative orientation of the nuclei (as specified by the angles Θ_1, Θ_2, and Φ) and any distance R between the nuclei. Further, we substitute the values found for the potential into Eq. (4) or (6) in order to determine the transmission coefficient for the chosen relative orientation of nuclei. After averaging over various relative spatial orientations of nuclei (3), we obtain the fusion cross section.

It was indicated above that, in calculating the fusion of two deformed nuclei, it is necessary to average the cross section over all possible relative orientations of colliding nuclei since, under experimental conditions, colliding nuclei may have various relative orientations. Different values of the barrier height and different shapes of both the potential barrier and the capture well correspond to different values of the angles Θ_1, Θ_2, and Φ. Therefore, it is interesting to investigate the effect of various approximations on the cross section—for example, the approximation where one ignores integration with respect to some angle (in particular, the angle Φ). It should be noted that averaging over the angle Φ is frequently disregarded in studying the subbarrier fusion of two deformed nuclei (see, for example, [9, 13, 14, 34]).

Nuclear quadrupole- and hexadecapole-deformation parameters used in the calculations of the fusion cross sections

Nucleus	β_{20}	β_{40}
^{24}Mg	0.438	0
^{28}Si	−0.407	0
^{48}Ca	0	0
^{50}Cr	0.293	0
^{58}Fe	0.2587	−0.019
^{150}Nd	0.2848	0.107
^{154}Sm	0.34	0
^{158}Gd	0.3484	0.079
^{238}U	0.2863	0.093
^{244}Pu	0.2931	0.062
^{248}Cm	0.2972	0.040

The cross section for the production of superheavy nuclei has a maximum at energies 5 to 10 MeV lower than the barrier energy obtained in our approximation (see [24, 25]). Because of this, we are interested in the capture cross sections for heavy nuclei in the vicinity of the barrier where the effect of the loss of kinetic energy at the initial stage of a collision event on the reaction cross section is small. The potential parametrization used in [34] and in previous studies of the same authors leads to a lower barrier height in relation to our estimates (see the details in [24]); therefore, the loss of kinetic energy at the initial stage of a collision event and coupling to other reaction channels are important in the approximation used in [34].

4. DISCUSSION OF THE RESULTS

First, we will study in detail the potentials and fusion cross sections for light and medium-mass nuclei and then address the case of heavy nucleus–nucleus systems. This partition of systems of colliding nuclei in mass is motivated by the fact that a compound nucleus is always formed after the barrier is

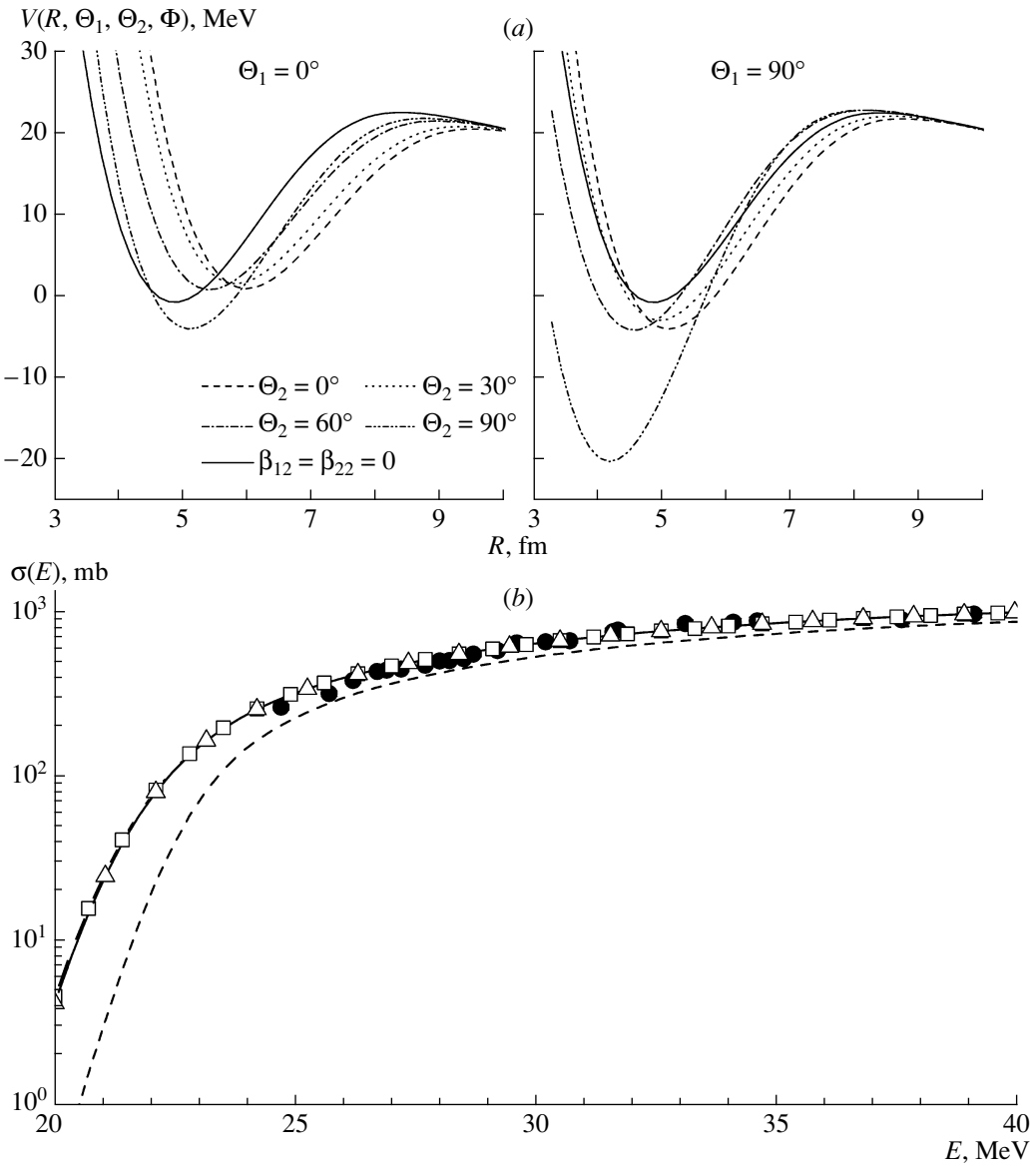

Fig. 2. (*a*) Total potential of the nuclear interaction in the $^{24}Mg + {}^{24}Mg$ system for various relative orientations of the nuclei involved. (*b*) Fusion cross section versus the energy for the $^{24}Mg + {}^{24}Mg$ reaction. The closed circles represent experimental data. The solid and dashed curves stand for the fusion cross section calculated, respectively, in the most accurate approximation and under the assumption that both nuclei are spherical. The open boxes and triangles correspond to the calculations, respectively, without the quadratic terms in the quadrupole deformation of both nuclei and without averaging over the angle Φ (these points are connected by lines in order to guide the eye).

overcome by colliding light and medium-mass nuclei. But in the case of heavy-ion collisions followed by the formation of two fused nuclei in a potential pocket after they have overcome the fusion barrier, the resulting nuclear system may evolve differently. A compound nucleus may arise, or the system may undergo breakup, skipping the compound-nucleus stage (quasifission)—see [24, 35, 36] and references therein. In the case of heavy nuclear systems, we will therefore analyze the cross section for the formation of a dinuclear system in a potential pocket (capture cross section). This cross section is also described by relations (3)–(6).

We will analyze available experimental data on the fusion of light and medium-mass deformed nuclei [37–39]. In the case where very heavy dinuclear systems are formed upon a collision of nuclei, experimental data on the capture cross section were obtained at several values of the collision energy for a deformed and a spherical nucleus [36]; for two deformed nuclei, these cross sections were measured at only one collision energy [36].

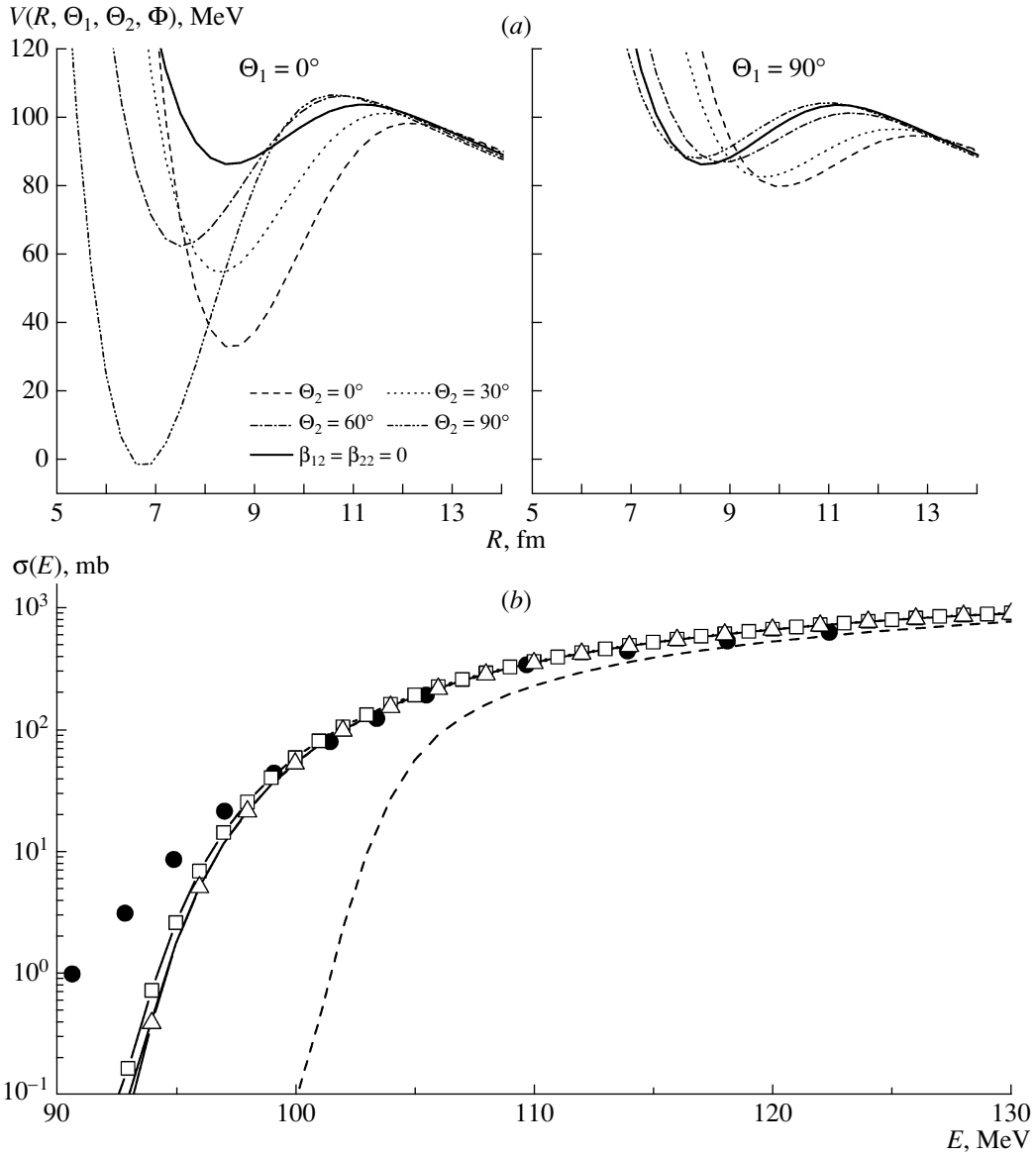

Fig. 3. (*a*) Total potential of the interaction in the the $^{154}Sm + ^{28}Si$ system for various relative orientations of the nuclei involved. (*b*) Fusion cross section versus energy for the $^{154}Sm + ^{28}Si$ reaction. The notation for the curves and points is identical to that in Fig. 2.

4.1. Cross Section for the Fusion of Light and Medium-Mass Nuclei

In order to clarify the role of the deformation type (prolate versus oblate) and the effect of the terms involving β_{12}^2, β_{22}^2, and $\beta_{12}\beta_{22}$ on the fusion cross section, we will consider in detail the $^{24}Mg + ^{24}Mg$ (both nuclei are prolate), $^{154}Sm + ^{28}Si$ (an prolate and an oblate nucleus), and $^{28}Si + ^{28}Si$ (two oblate nuclei) fusion reactions. The experimental values of the quadrupole deformations for these nuclei were borrowed from [40] and are presented here in the table. In Figs. 2*a*, 3*a*, and 4*a*, we show potentials for characteristic relative orientations of the nuclei, while, in Figs. 2*b*, 3*b*, and 4*b*, we compare fusion cross sections calculated in various approximations and experimental data [37–39].

A good description of experimental fusion cross sections at energies above the barrier was attained by varying the parameter η [see Eq. (5)]. A variation in η leads to a change in the barrier height and position, and this makes it possible to fit readily the cross section at high energies. However, the cross section at subbarrier energies depends greatly on taking into account various mechanisms of tunneling through the barrier and on the accuracy in calculating the potential. We have determined the following values

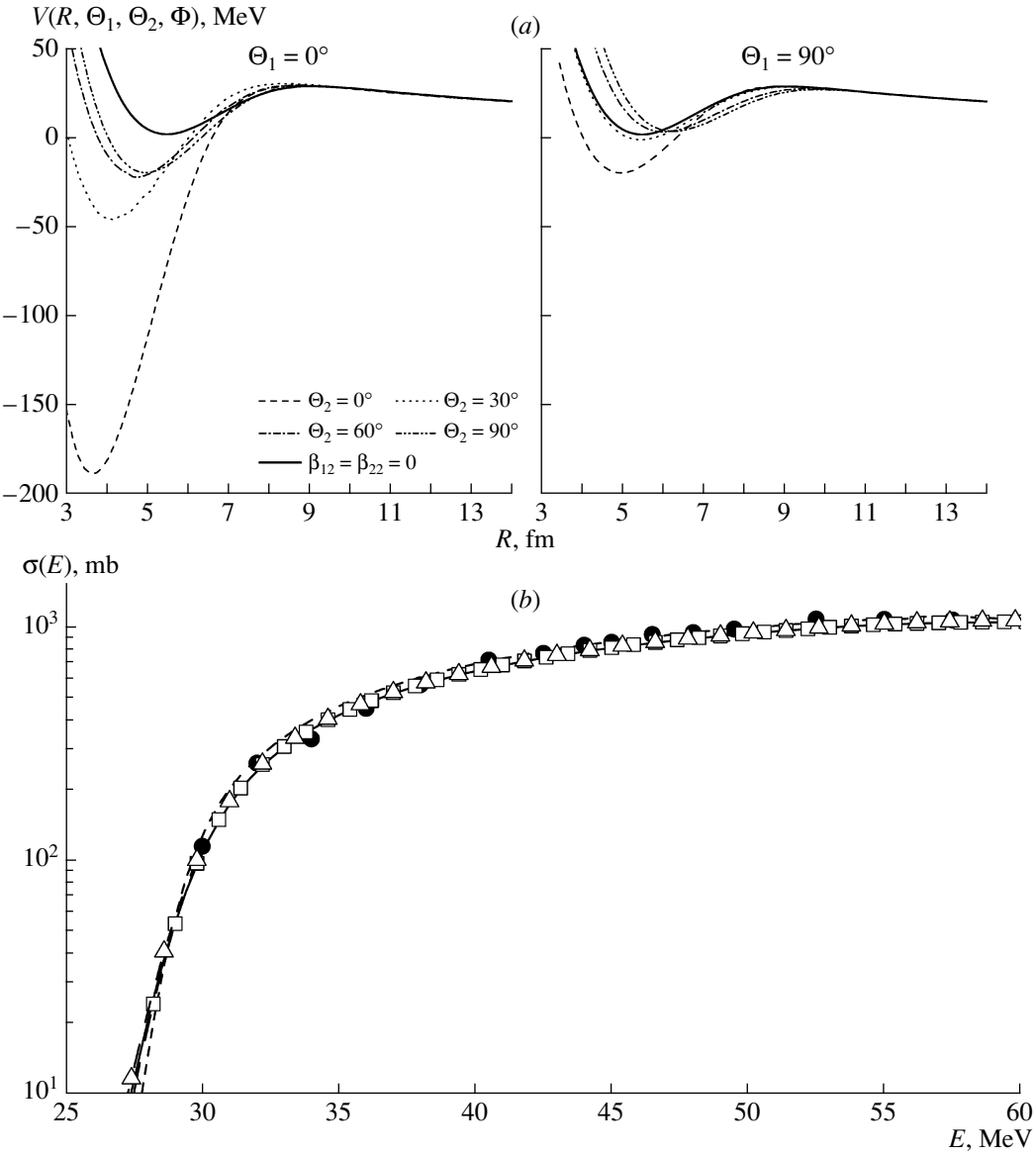

Fig. 4. (*a*) Total potential of the interaction in the $^{28}Si + {}^{28}Si$ system for various relative orientations of the nuclei involved. (*b*) Fusion cross section versus energy for the $^{28}Si + {}^{28}Si$ reaction. The notation for the curves and points is identical to that in Fig. 2.

for the $^{24}Mg + {}^{24}Mg$, $^{154}Sm + {}^{28}Si$, and $^{28}Si + {}^{28}Si$ reactions: $\eta = 0.95$, 0.96, and 0.955.

In Figs. 2–4, we present the fusion cross sections calculated in the approximation of spherical nuclei. This approximation makes it possible to describe the fusion cross section at high energies (above the barrier), but, at subbarrier energies, it underestimates strongly experimental data for the $^{24}Mg + {}^{24}Mg$ and $^{154}Sm + {}^{28}Si$ systems. Upon taking into account the deformations of colliding nuclei, the subbarier-fusion cross section increases considerably, which improves substantially the description of experimental data over the entire energy range being considered.

For the $^{24}Mg + {}^{24}Mg$ and $^{28}Si + {}^{28}Si$ systems, which are quite light, the effect of second-order terms in the quadrupole deformation on the fusion cross section cannot be traced, while, for the $^{154}Sm + {}^{28}Si$ system, it is insignificant. For all systems, variations in the orientation angle Φ do not lead to any sizable effect.

The above features in the behavior of the fusion cross section follow from the dependence that we presented for the total nucleus–nucleus potential in the case of various orientations of nuclei. From Fig. 4, one can see that variations in the orientation of light oblate nuclei forming the $^{28}Si + {}^{28}Si$ system lead to insignificant variations in the barrier height; therefore,

the cross sections calculated for spherical nuclei are close to the cross sections found in our most precise approximation, which takes into account the deformations of nuclei and averaging over all angles. In contrast to the results obtained in this case, substantial changes in the barrier height in response to variations in the angles Θ_1 and Θ_2 can clearly be seen in Fig. 2 and especially in Fig. 3. By way of example, we indicate that, in the case where the orientation of the nuclei in the $^{24}Mg + {}^{24}Mg$ system is specified by the angles of $\Theta_1 = \Theta_2 = 0°$, the barrier height is less than that in the case of spherical nuclei by several MeV units. This dependence of the barrier height on the relative orientation of nuclei leads to a sizable increase in the cross section for subbarrier energies. For the $^{154}Sm + {}^{28}Si$ system, the barrier is the lowest at $\Theta_1 = 0°$ and $\Theta_1 = 90°$. We note that it is lower than that in the case of the respective spherical nuclei by about 9 MeV, and this is the reason for a significant increase in the fusion cross section in the region of low energies.

In describing the aforementioned reactions, it is of paramount importance to take into account averaging over the angles Θ_1 and Θ_2. If the averaging over these angles were not performed, the fusion cross section determined, for example, in the case of the orientation corresponding to the maximum barrier height would be smaller than the cross section calculated in the approximation of spherical nuclei.

As was shown in [25], a variation in the angle Φ leads to sizable changes in the barrier height for the case of heavy nuclear systems; therefore, the effect of averaging over the angle Φ on the fusion cross sections is insignificant for light and medium-mass nuclear systems (see Figs. 2–4).

4.2. Capture Cross Section for Heavy Nuclei

Capture cross sections for heavy nucleus–nucleus systems are of particular interest since the synthesis of superheavy elements occurs in these reactions [26] and since this capture process resulting in the formation of a system of fused touching nuclei is the initial stage of the process of superheavy-element formation [24, 35, 36].

The experimental capture cross sections were measured by Itkis et al. [36] for asymmetric nuclear systems. Therefore, we begin our analysis by considering the capture cross section in the case of a collision between mass-asymmetric nuclei. Unfortunately, experimental data are available only for a limited set of reactions and energies. We will analyze the entire set of available data. We will first consider mass-asymmetric reactions between a spherical and a deformed nucleus and then investigate the capture cross section in a collision between deformed nuclei.

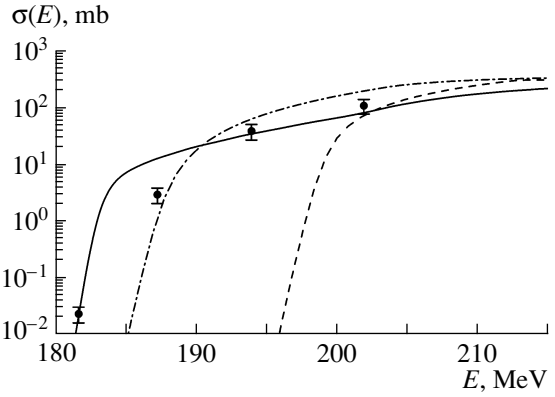

Fig. 5. Capture cross section as a function of energy for the $^{48}Ca + {}^{238}U$ reaction: experimental data (points) and results of calculations (curves) in the most precise approximation (solid curve), in the approximation where both nuclei are spherical (dashed curve), and without allowance for the hexadecapole deformation of the nuclei (dash-dotted curve).

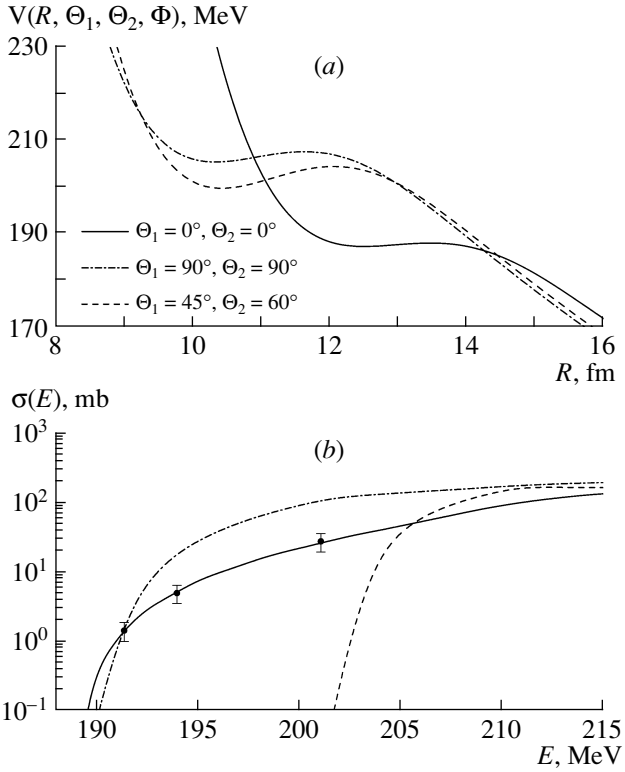

Fig. 6. (*a*) Total potential of the interaction between the nuclei in the $^{48}Ca + {}^{244}Pu$ system for various relative orientations of its constituents. (*b*) Capture cross section as a function of energy for the $^{48}Ca + {}^{244}Pu$ reaction (the notation is identical to that in Fig. 5).

It is also of interest to study the capture cross section for nuclei close in mass. A characteristic example of such a reaction is given at the end of Section 4.2.

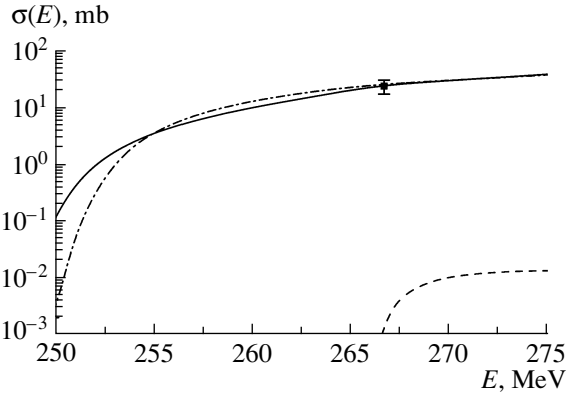

Fig. 7. Capture cross section as a function of energy for the $^{58}Fe + {}^{248}Cm$ reaction. The notation is identical to that in Fig. 5.

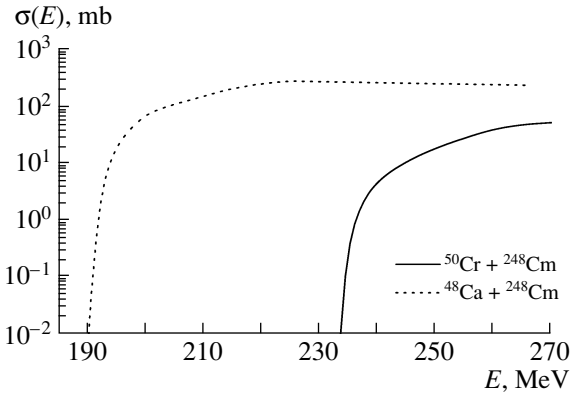

Fig. 8. Capture cross section as a function of energy for the $^{48}Ca + {}^{248}Cm$ and $^{50}Cr + {}^{248}Cm$ reactions.

Collisions of mass-asymmetric nuclei. In Figs. 5, 6, and 7, we compare the results of the calculations with experimental data on the capture cross sections for the $^{48}Ca + {}^{238}U$, $^{48}Ca + {}^{244}Pu$, and $^{58}Fe + {}^{248}Cm$ reactions, respectively. The cross sections calculated with allowance for the second-order terms in the quadrupole and hexadecapole deformations of the ^{238}U, ^{244}Pu, ^{58}Fe, and ^{248}Cm nuclei agree well with experimental data. The experimental values of the quadrupole deformation for these nuclei were borrowed from [40], and the hexadecapole-deformation values used here were calculated in [41]. These parameter values are presented in the table. For the $^{48}Ca + {}^{238}U$, $^{48}Ca + {}^{244}Pu$, and $^{58}Fe + {}^{248}Cm$ reactions, we employed the η values of $\eta = 0.94, 0.894$, and 0.96, respectively.

In the approximation where colliding nuclei are spherical, the experimental values of the capture cross section are significantly underestimated. This underestimation of the capture cross section may be due to the fact that the potential-barrier height calculated for spherical nuclei exceeds the barrier height calculated with allowance for deformation of the heavy nucleus whose orientation is specified by an angle of $\Theta_1 = 0°$ (see Fig. 6*a*). Moreover, the potential well calculated in the spherical-nucleus approximation is shallower than the potential well calculated with allowance for the deformation of nuclei. Therefore, the well can capture a smaller number of partial waves, and this leads to a decrease in the cross section even at high energies. This effect is the most pronounced in the $^{58}Fe + {}^{248}Cm$ reaction: at high energies, the capture cross section for this reaction is an order of magnitude smaller than the capture cross sections for the $^{48}Ca + {}^{238}U$ and $^{48}Ca + {}^{244}Pu$ reactions. We also note than the hexadecapole deformation of the ^{248}Cm nucleus is smaller than that of the ^{238}U and ^{244}Pu nuclei.

Although the hexadecapole deformation is small in heavy nuclei, its inclusion has a significant effect on cross-section values, especially at low energies (see Figs. 5–7). This is because the hexadecapole deformation affects the barrier height and changes significantly the depth of the capture well for some orientations of nuclei.

In [34], $^{48}Ca + {}^{238}U$ and $^{48}Ca + {}^{244}Pu$ capture cross sections close to our values were obtained at collision energies corresponding to the maximum yield of three neutrons from the compound nucleus. No hexadecapole deformation of nuclei was taken into account there, but a different parametrization of the nuclear component of the interaction between the nuclei was used.

We note that, as the mass and the charge of colliding nuclei increase, the depth of the well decreases [24, 25]. This leads to a decrease in the capture cross section; for especially heavy systems, the capture cross section vanishes because there is no capture well in the potential. For example, the capture cross section for the $^{76}Se + {}^{244}Pu$ reaction is smaller than that for the lighter $^{58}Fe + {}^{248}Cm$ system, and the accuracy in calculating the potential and the role of the hexadecapole deformations are of paramount importance for evaluating cross sections.

The ^{50}Cr nucleus is a strongly deformed even–even nucleus. It is convenient to use this nucleus—in the same way as the ^{48}Ca nucleus—for experiments devoted to synthesizing superheavy nuclei. In planning future experiments in this field, it is therefore of interest to compare the cross sections for capture on two neighboring nuclei (^{48}Ca and ^{50}Cr) and on the same heavy target nucleus (^{248}Cm). We note that the ^{50}Cr nucleus has a significant quadrupole deformation in contrast to the spherical doubly magic ^{48}Ca nucleus. Figure 8 shows the capture cross sections for the $^{48}Ca + {}^{248}Cm$ and $^{50}Cr + {}^{248}Cm$

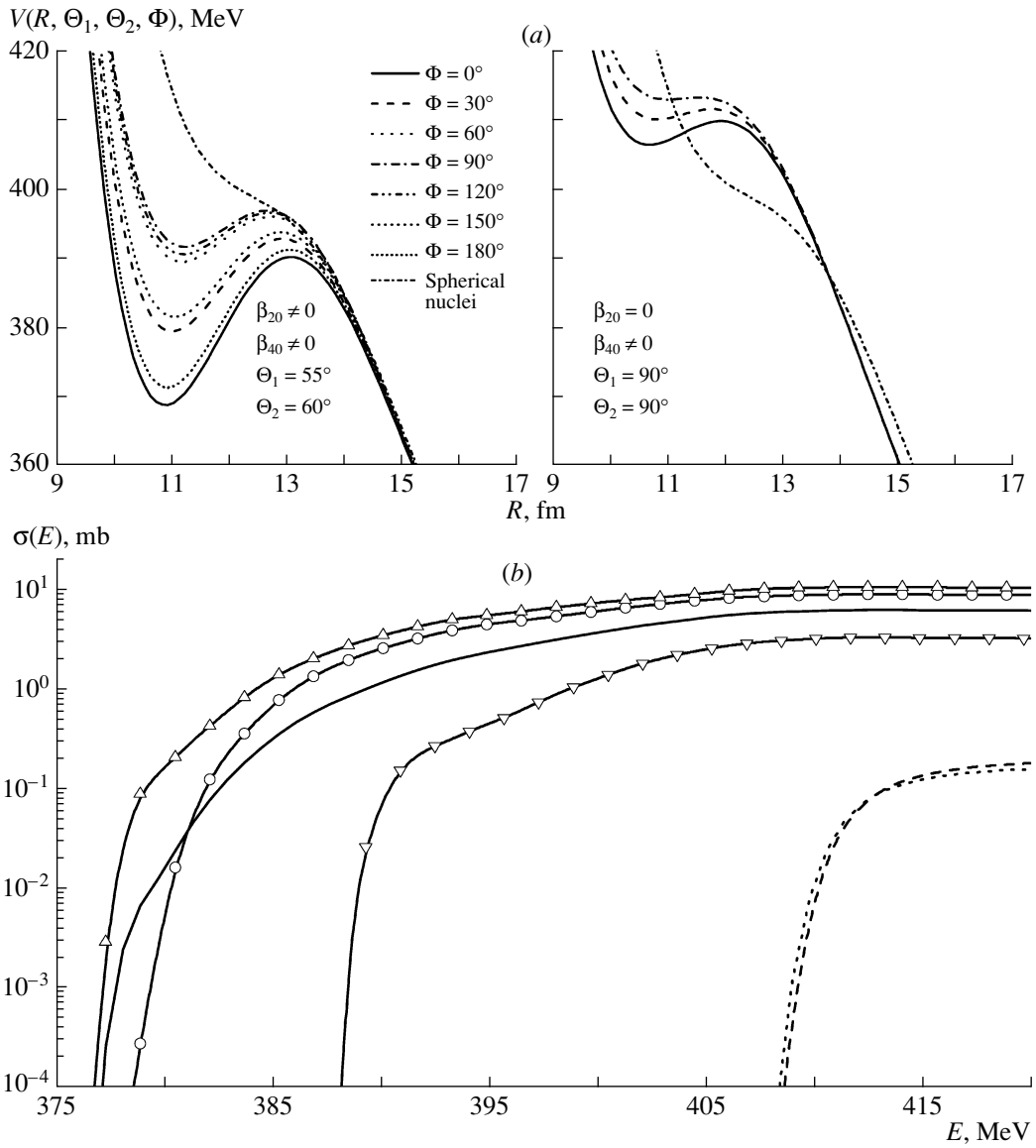

Fig. 9. (*a*) Total potential of the interaction between the nuclei in the $^{150}Nd + {}^{158}Gd$ system for their various relative orientations associated with the angle Φ. The angles Θ_1 and Θ_2 were chosen in such a way that the depth of the potential capture well is maximal. The potential for spherical nuclei is presented for the sake of comparison. (*b*) Fusion cross section as a function of energy for the $^{150}Nd + {}^{158}Gd$ reaction according to various versions of the calculations. All versions of the calculations involve averaging over the angles Θ_1 and Θ_2. The solid, dotted, and dashed curves represent the fusion cross section calculated, respectively, in the most accurate approximation, without allowance for the hexadecapole deformation, and without allowance for quadratic terms in the quadrupole deformation and linear terms in the hexadecapole deformation. The points represent the results for the fusion cross section calculated at $\Phi =$ (open triangles) 0°, (open inverted triangles) 90°, and (open circles) 180°.

reactions according to the calculations performed at $\eta = 0.94$. The capture cross sections calculated for the $^{48}Ca + {}^{248}Cm$ reaction in the high-energy region are one order of magnitude larger the corresponding values for the $^{50}Cr + {}^{248}Cm$ reaction. However, the capture cross sections for the $^{50}Cr + {}^{248}Cm$ and $^{58}Fe + {}^{248}Cm$ reactions are close to each other (see Figs. 7 and 8). Making a rough assumption that the stages of the superheavy-element synthesis that follow capture in $^{48}Ca + {}^{248}Cm \Rightarrow {}^{296-x}116 + xn$, $^{50}Cr + {}^{248}Cm \Rightarrow {}^{298-x}120 + xn$, and $^{58}Fe + {}^{248}Cm \Rightarrow {}^{306-x}122 + xn$ collisions are identical, we find that the cross section for the production of the element 116 is one order of magnitude larger than the cross section for the production of the elements 120 and 122; that is, it is about 0.1 pb. Here, we consider that the experimentally measured value of the cross

section for the production of the element 116 is about 1 pb [26].

If the same superheavy nucleus (with $Z \gtrsim 120$) can be synthesized in collisions of different isotopes of target and projectile nuclei, a colliding system that consists of more deformed target and projectile nuclei is preferable because it may have a deeper capture well for some orientations of colliding nuclei; therefore, it may have a larger capture cross section.

Collisions of nuclei close in mass. In the case of collisions between nuclei that are close in mass (such collisions lead to the production of a very heavy nuclear systems), the depth of the well and the capture cross section decrease [24]. For the two strongly deformed nuclei in the $^{150}\mathrm{Nd} + {}^{158}\mathrm{Gd}$ system, the nucleus–nucleus potential for various relative orientations of the nuclei is given in Fig. 9 along with the capture cross section calculated in various approaches. The values of the deformations for these nuclei were borrowed from [40] and are given in the table. This reaction may lead to the production of an element involving 124 protons.

The nucleus–nucleus potentials are depicted in Fig. 9 at values of the angles Θ_1 and Θ_2 such that the potentials possess the maximum depth of the capture well. With allowance for the hexadecapole deformation, these angles are $\Theta_1 = 55^\circ$ and $\Theta_2 = 60^\circ$. At the same time, these angles are $\Theta_1 = \Theta_2 = 90^\circ$ if the hexadecapole deformation is not taken into account. In either case, the depth of the capture well reaches a maximum at an angle of $\Phi = 0^\circ$.

In the spherical-nucleus approximation, the nucleus–nucleus potential for the $^{150}\mathrm{Nd} + {}^{158}\mathrm{Gd}$ system does not have a potential well (Fig. 9); therefore, the capture cross section vanishes in this approximation.

For such heavy and almost symmetric systems, it is of paramount importance to take into account the hexadecapole deformation and to perform averaging over all angles describing the relative orientation of nuclei in calculating both the potential and the fusion cross section. Figure 9*a* gives the results obtained for the potentials with (right panel) and without (left panel) hexadecapole deformation. The inclusion of the hexadecapole deformation leads to a sizable increase in the depth of the potential well at some relative orientations of the nuclei and, hence, to an increase in the number of captured partial waves. This dependence of the potential on the hexadecapole deformation is also reflected in the capture cross section. As a result, the cross sections calculated with and without allowance for the hexadecapole deformation differ very strongly (see Fig. 9*b*).

The dependence of the potential on the angle Φ is also quite pronounced. Analyzing the behavior of the curves in Fig. 9, we note that the barrier height and the depth of the well depend significantly on the angle Φ. The dependence of the depth of the potential well on the angle Φ is responsible for different values of the capture cross section at above-barrier energies; at the same time, the dependence of the the fusion-barrier height on the angle Φ manifests itself at low energies. If the hexadecapole deformation is taken into account, the symmetry axes of nuclei are nearly parallel at $\Phi = 0^\circ$, because $\Theta_1 = 55^\circ \approx \Theta_2 = 60^\circ$ in this case. But at $\Phi = 180^\circ$, the symmetry axes of the nuclei are nearly orthogonal. As a result, the potentials calculated at $\Phi = 0^\circ$ and $\Phi = 180^\circ$ or at $\Phi = 30^\circ$ and $\Phi = 150^\circ$ are different.

The effect of averaging over the angle Φ on the capture cross section is studied by fixing some values of the angle Φ. Choosing the values of $\Phi = 0^\circ, 90^\circ$, and 180°, for example, and not performing averaging over Φ, we obtained different values of the cross section (see Fig. 9). The capture cross section calculated at $\Phi = 0^\circ$ is maximal and exceeds the values obtained by means of our precise calculation. However, the capture cross section calculated for the orientation corresponding to $\Phi = 90^\circ$ is underestimated in relation to the values obtained from the precise calculations.

We have investigated in detail the dependence of the capture cross section on the angle Φ, because we deemed that the importance of averaging over the angles Θ_1 and Θ_2 is obvious.

If we neglect the hexadecapole deformation of nuclei, the inclusion in the nucleus–nucleus potential of quadratic terms in the quadrupole deformation leads to insignificant variations in this potential in relation to the potential calculated with allowance for only linear terms in the quadruple deformation. Therefore, the capture cross section also changes only slightly in these cases (see Fig. 9). We note, however, that $\beta_2^2 \approx \beta_{L>2}$; therefore, it is necessary to take into account β_2^2 terms as well in a consistent accurate calculation of both the potential and the capture cross section with allowance for the hexadecapole deformation.

5. CONCLUSIONS

To summarize, we list our basic results.

(1) Variations in the relative orientation of deformed nuclei change significantly the barrier height, the barrier position, the depth of the capture well, and the shape of the nuclear potential.

(2) For light nuclear systems, the effect of quadratic terms in the quadrupole deformation in the nuclear potential and the effect of averaging over the angle Φ are small. As the charges and the masses of colliding nuclei increase, averaging over the angle Φ affects

more strongly both the capture (fusion) cross section at subbarrier energies and the barrier height.

(3) A prolate deformation of the nucleus affects most strongly both the nuclear potential and the capture (fusion) cross section in the case of light and heavy nuclei. An oblate deformation of the nucleus has an effect both on the nucleus–nucleus potential and on the capture (fusion) cross section for heavy nuclear systems.

(4) The inclusion of a hexadecapole deformation is of particular importance in calculating the capture cross section in heavy nuclear systems. The reason for this is that a hexadecapole deformation leads to a significant increase in the well depth at some relative orientations of colliding nuclei.

REFERENCES

1. P. E. Hodgson, *Nuclear Heavy-Ion Reactions* (Oxford Univ., Oxford, 1978).
2. R. Bass, *Nuclear Reactions with Heavy Ions* (Springer, Berlin, 1980).
3. W. Nörenberg and H. A. Weidenmüller, *Introduction to the Theory of Heavy-Ion Collisions* (Springer, Berlin, 1980).
4. G. R. Satchler, *Direct Nuclear Reactions* (Oxford Univ., Oxford, 1983).
5. H. Feshbach, *Theoretical Nuclear Physics: Nuclear Reactions* (Wiley, New York, 1992).
6. P. Fröbrich and R. Lipperheide, *Theory of Nuclear Reactions* (Oxford Univ., Oxford, 1996).
7. G. Wallerstein et al., Rev. Mod. Phys. **69**, 995 (1997).
8. V. Yu. Denisov, Phys. Rev. C **74**, 055804 (2006).
9. C. Y. Wong, Phys. Rev. Lett. **31**, 766 (1973).
10. L. C. Vaz, J. M. Alexander, and G. R. Satchler, Phys. Rep. **69**, 373 (1981).
11. M. Beckermann, Phys. Rep. **129**, 145 (1985); Rep. Prog. Phys. **51**, 1047 (1988).
12. V. P. Permyakov and V. M. Shilov, Sov. J. Part. Nucl. **20**, 594 (1989).
13. J. O. Fernandez-Niello, C. H. Dasso, and S. Landowne, Comput. Phys. Commun. **54**, 409 (1989).
14. C. H. Dasso, J. Fernandez-Niello, and S. Landowne, Phys. Rev. C **41**, 1014 (1990).
15. V. Yu. Denisov, Yad. Fiz. **54**, 1556 (1991) [Sov. J. Nucl. Phys. **54**, 952 (1991)].
16. V. Yu. Denisov and G. Royer, J. Phys. G **20**, L43 (1994).
17. W. Reisdorf, J. Phys. G **20**, 1297 (1994).
18. V. Yu. Denisov and G. Royer, Yad. Fiz. **58**, 448 (1995) [Phys. At. Nucl. **58**, 397 (1995)].
19. V. Yu. Denisov and S. V. Reshit'ko, Yad. Fiz. **59**, 78 (1996) [Phys. At. Nucl. **59**, 72 (1996)].
20. A. B. Balantekin and N. Takigawa, Rev. Mod. Phys. **70**, 77 (1998).
21. M. Dasgupta, D. J. Hinde, N. Rowley, and A. M. Stefanini, Annu. Rev. Nucl. Part. Sci. **48**, 401 (1998).
22. V. Yu. Denisov, Yad. Fiz. **62**, 1431 (1999) [Phys. At. Nucl. **62**, 1349 (1999)]; V. Yu. Denisov, Eur. Phys. J. A **7**, 87 (2000).
23. I. I. Gontchar et al., Phys. Rev. C **65**, 034610 (2002).
24. V. Yu. Denisov and W. Nörenberg, Eur. Phys. J. A **15**, 375 (2002); V. Yu. Denisov, Eur. Phys. J. A **25** (Suppl. 1), 619 (2005).
25. V. Yu. Denisov and N. A. Pilipenko, Phys. Rev. C **76**, 014602 (2007); Ukr. J. Phys. **53**, 845 (2008).
26. Yu. Ts. Oganessian, J. Phys. G **34**, R165 (2007).
27. V. Yu. Denisov, Phys. Lett. B **526**, 315 (2002).
28. V. Yu. Denisov, AIP Conf. Proc. **704**, 92 (2004).
29. J. Blocki, J. Randrup, W. J. Swiatecki, and C. F. Tsang, Ann. Phys. (N.Y.) **105**, 427 (1977).
30. J. Randrup and J. S. Vaagen, Phys. Lett. B **77**, 170 (1978).
31. V. Yu. Denisov, Yad. Fiz. **51**, 1263 (1990) [Sov. J. Nucl. Phys. **51**, 803 (1990)].
32. L. D. Landau and E. M. Lifshitz, *Course of Theoretical Physics,* Vol. 3: *Quantum Mechanics: Non-Relativistic Theory* (Nauka, Moscow, 1989, 4th ed.; Pergamon, Oxford, 1977, 3rd ed.).
33. D. L. Hill and J. A. Wheeler, Phys. Rev. **89**, 1102 (1953).
34. V. V. Sargsyan et al., Yad. Fiz. **72**, 459 (2009) [Phys. At. Nucl. **72**, 425 (2009)]; G. G. Adamian, N. V. Antonenko, and V. V. Sargsyan, Phys. Rev. C **79**, 054608 (2009).
35. V. Yu. Denisov and S. Hofmann, Phys. Rev. C **61**, 034606 (2000).
36. M. G. Itkis et al., in *Proc. of the Intern. Workshop on Fusion Dynamics at the Extremes, Dubna, 2000*, Ed. by Yu. Ts. Oganessian and V. I. Zagrebaev (World Sci., Singapore, 2001), p. 93; J. Nucl. Radiochem. Sci. **3**, 57 (2002); Nucl. Phys. A **734**, 136 (2004); AIP Conf. Proc. **853**, 231 (2006); Nucl. Phys. A **787**, 160 (2007).
37. C. M. Jachcinski et al., Phys. Rev. C **24**, 2070 (1981).
38. S. Gil et al., Phys. Rev. Lett. **65**, 3110 (1990).
39. Y. Nagashima et al., Phys. Rev. C **33**, 33 (1986).
40. http://cdfe.sinp.msu.ru/services/radchart/radmain.html
41. P. Möller, J. R. Nix, W. D. Myers, and W. J. Swiatecki, At. Data Nucl. Data Tables **59**, 195 (1995).

Translated by A. Isaakyan